

Size-Dependent Surface Reactions of Ag Nanoparticles Supported on Highly Oriented Pyrolytic Graphite

Hui Zhang, Qiang Fu,* Yunxi Yao, Zhen Zhang, Teng Ma, Dali Tan, and Xinhe Bao*

State Key Laboratory of Catalysis, Dalian Institute of Chemical Physics, The Chinese Academy of Sciences, Dalian 116023, People's Republic of China

Received December 12, 2007. Revised Manuscript Received June 24, 2008

Various sizes of Ag particles were grown on highly oriented pyrolytic graphite (HOPG) surfaces, which had previously been modified with nanopits to act as anchoring sites. Surface reactions of O₂, CHCl₃, and CCl₄ on the Ag particles and bulk Ag(111) surfaces were studied by X-ray photoelectron spectroscopy (XPS), and it has been shown that size dependence of O₂ and CHCl₃ reactions on Ag differs from that of CCl₄. Weak reactions of O₂ and CHCl₃ were observed on the bulk Ag(111) surfaces, while strong reactions occur on Ag particles with medium Ag coverage, suggesting that the reactions are controlled by the number of surface defect sites. On the contrary, the dissociation of CCl₄ is mainly determined by the exposed Ag facet area, mainly Ag(111) facet, and strong dissociation reaction happens on the bulk Ag(111) surface. The results suggest that the size effects, which are often discussed in heterogeneous catalysis, are strongly dependent on the reaction mechanism.

1. Introduction

Supported metal particles often demonstrate size-dependent catalytic properties, and various size effects in the heterogeneous catalysis have been extensively addressed in past decades.¹ First, nanoparticles present multiple low coordination surface atoms, such as facets, edges, corners, and defects, which have been regarded as the highly active sites for some surface reactions.² Second, interfacial atoms that interact with the support surface could be crucial to catalytic reactions due to the interfacial interaction and corresponding charge transfer between metal and support.^{3–5} Finally, spatial confinement in nanoparticles causes quantum size effects, which lead to the formation of discrete electron levels and change dramatically the catalytic properties of the metal nanoparticles.^{6–8}

Moreover, reactivity of the metal nanoparticles depends on the surface adsorbates, which may show affinity for particular reaction sites.⁹ Structure-sensitive reactions can be orders of magnitude faster on favorable sites over the unfavorable ones. As mentioned above, nanoparticles exhibit various active surface sites, which make it possible to observe size-dependent catalytic properties of metal nanoparticles for the structure-sensitive reactions. On the other hand, the structure-insensitive reactions are carried out at a similar rate on many different surface sites, and the size effects may play little role in these catalytic reactions.

One of the commonly studied metal nanoparticle catalysts has been Ag, which plays a critical role in the selective oxidation of ethylene to ethylene oxide as well as the oxidation of methanol

to formaldehyde.^{10–14} Many surface studies using Ag catalysts have been focused on Ag particles grown on oxide surfaces where the metal–oxide interaction and the oxide support surfaces could affect the surface catalytic reactions.¹⁵ It would therefore be interesting to find a system where the support exhibits weak coupling to the adsorbate as well as the metal nanoparticles to remove the influence of the support. Highly oriented pyrolytic graphite (HOPG) is such a material. For many adsorbate reactions, the interaction between the Ag metal and HOPG is very weak.^{16,17} This system, where Ag nanoparticles are supported on HOPG, may present the intrinsic catalytic properties of the metal particles and provide a suitable playground for studies in the size effects where the role of the support is minimized.

In the present study, Ag particles were deposited onto HOPG. The size of the Ag particles was controlled through modification of the HOPG surfaces with nanopits as well as the Ag evaporation time. The reactions of O₂, CHCl₃, and CCl₄ to the Ag particles and bulk Ag(111) surfaces were studied by X-ray photoelectron spectroscopy (XPS). It has been shown that the size dependence of O₂ and CHCl₃ reactions on Ag differs from that of CCl₄ reactions, which suggest different mechanisms dominating the different size-dependent reactions.

2. Experimental Section

An Omicron multiprobe surface analysis system was used for the surface experiments. It has been described in detail elsewhere^{7,18} and will be summarized shortly here. It consisted of three ultrahigh vacuum (UHV) chambers. The first chamber was used to prepare the surface by a cleaning/deposition cycle. The surface was then

* Corresponding author. Phone: +86-411-84686637. Fax: +86-411-84694447. E-mail: xhbao@dicp.ac.cn (X.B.); qfu@dicp.ac.cn (Q.F.).

(1) Chen, M. S.; Goodman, D. W. *Acc. Chem. Res.* **2006**, *39*, 739.
(2) Schalow, T.; Brandt, B.; Starr, D. E.; Laurin, M.; Shaikhutdinov, S. K.; Schauermann, S.; Libuda, J.; Freund, H. J. *Angew. Chem., Int. Ed.* **2006**, *45*, 3693.
(3) Chen, M. S.; Goodman, D. W. *Science* **2004**, *306*, 252.
(4) Lemire, C.; Meyer, R.; Shaikhutdinov, S.; Freund, H. J. *Angew. Chem., Int. Ed.* **2004**, *43*, 118.
(5) Fu, Q.; Wagner, T. *Surf. Sci. Rep.* **2007**, *62*, 431.
(6) Valden, M.; Lai, X.; Goodman, D. W. *Science* **1998**, *281*, 1647.
(7) Zhang, Z.; Fu, Q.; Zhang, H.; Li, Y.; Yao, Y. X.; Tan, D.; Bao, X. H. *J. Phys. Chem. C* **2007**, *111*, 13524.
(8) Heiz, U.; Sanchez, A.; Abbet, S.; Schneider, W. D. *J. Am. Chem. Soc.* **1999**, *121*, 3214.
(9) Somorjai, G. A.; Park, J. Y. *Catal. Lett.* **2007**, *115*, 87.

(10) Mao, C. F.; Vannice, M. A. *Appl. Catal., A* **1995**, *122*, 61.
(11) Bulushev, D. A.; Paukshitis, E. A.; Nogin, Y. N.; Balzhinimaev, B. S. *Appl. Catal., A* **1995**, *123*, 301.
(12) Bukhtiyarov, V. I.; Prosvirin, I. P.; Kvon, R. I.; Goncharova, S. N.; Balzhinimaev, B. S. *J. Chem. Soc., Faraday Trans.* **1997**, *93*, 2323.
(13) Mao, C. F.; Vannice, M. A. *J. Catal.* **1995**, *154*, 230.
(14) Lee, J. K.; Vergyios, X. E.; Pitchai, R. *Appl. Catal.* **1989**, *50*, 171.
(15) Kim, Y. D.; Stultz, J.; Wei, T.; Goodman, D. W. *J. Phys. Chem. B* **2002**, *106*, 6827.
(16) Lopez-Salido, I.; Lim, D. C.; Dietsche, R.; Bertram, N.; Kim, Y. D. *J. Phys. Chem. B* **2006**, *110*, 1128.
(17) Hovel, H.; Barke, I. *Prog. Surf. Sci.* **2006**, *81*, 53.
(18) Jiang, Z. Q.; Huang, W. X.; Zhang, Z.; Zhao, H.; Tan, D. L.; Bao, X. H. *J. Phys. Chem. B* **2006**, *110*, 26105.

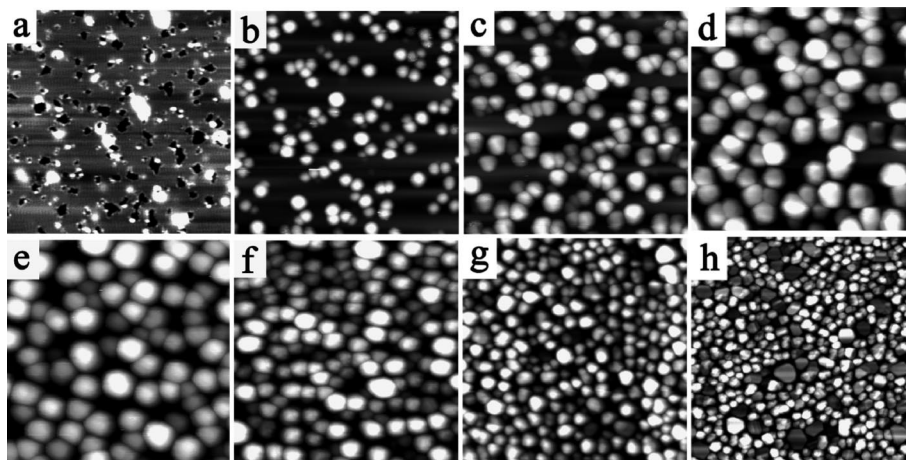


Figure 1. STM images of (a) the bare etched HOPG surface (100 nm \times 100 nm), and the Ag overlayers grown on HOPG with coverage of (b) 0.13 ML Ag (100 nm \times 100 nm), (c) 0.4 ML Ag (100 nm \times 100 nm), (d) 1.2 ML Ag (100 nm \times 100 nm), (e) 2 ML Ag (100 nm \times 100 nm), (f) 6 ML Ag (200 nm \times 200 nm), (g) 24 ML Ag (500 nm \times 500 nm), and (h) 48 ML Ag (1000 nm \times 1000 nm).

moved into the second chamber where it could be analyzed by XPS utilizing Mg K α ($h\nu = 1253.6$ eV) radiation with a pass energy of 30 eV. Finally, the surface was scanned by scanning tunneling microscopy (STM) in the third chamber with a room temperature (RT) apparatus under constant current mode using a homemade W-tip to look at the surface morphology.

To prepare the surface, the HOPG samples were cleaved with adhesive tape on a benchtop and were then loaded into the UHV preparation chamber. There, the HOPG samples were heated at 500 K for 10–15 min followed by bombardment with 500 V Ar $^+$ ions at 2.0×10^{-6} mbar for 3–6 min. The sputtered HOPG samples were then removed from the vacuum, oxidized in air at 560 $^{\circ}$ C for 10–12 min, and then returned to the UHV chamber. Before Ag deposition, the HOPG surfaces were heated to 900 K for half an hour to remove the surface impurities.

Once the surface was cleaned, Ag evaporation was performed in the preparation chamber using an effusion cell with the substrate at RT. The Ag coverage was controlled by manipulation of the deposition conditions, primarily the temperature of the Ag evaporator and the evaporation time. The flux of the Ag source was calibrated by measuring the monolayer formation of Ag on Si(111) because it is known that one monolayer (ML) of Ag on Si(111)-7 \times 7 produces a well-defined $\sqrt{3} \times \sqrt{3}$ -Ag-Si(111) structure as revealed by STM.¹⁹ Provided we know the deposition time and the temperature for our experiments, we can calculate the coverage.

Single crystal Ag(111) was used for comparison with the deposited Ag particles. The surfaces were cleaned by repeated Ar $^+$ sputtering (1000 eV, 15 μ A, 300 s) and UHV annealing (700 K, 300 s) until no contaminants were detected by XPS. STM shows that the Ag(111) surface was atomically flat after this procedure.

The introduction of adsorbates to the Ag surfaces was carried out by backfilling the chamber with CCl $_4$, CHCl $_3$, or O $_2$ using a leak valve. The pressure rise in the chamber as well as the time of exposure was used to calculate the coverage in Langmuir. The CCl $_4$ and CHCl $_3$ were purified by multiple freeze–pump–thaw cycles.

3. Results and Discussion

3.1. Preparation of Ag/HOPG. Because of the weak interaction between the metal and a pristine HOPG surface, metal adatoms tend to diffuse to surface steps where they aggregate into large particles. Furthermore, the easy tip-induced movement of metal particles on the defect-free HOPG surfaces makes it difficult to acquire reliable STM images. As a consequence, the surface defects on HOPG could act as anchoring sites for nucleation and growth of metal nanoparticles. The density of

natural defects on the HOPG surface is quite low,²⁰ so it is necessary to create surface defects. A two-step process consisting of Ar $^+$ sputtering in UHV followed by annealing in air has been widely applied to produce nanopits on HOPG surfaces.^{20–23} The result of this process is shown in Figure 1a. Here, we see a typical STM image of the HOPG surface subjected to the two-step preparation process, and it is clear that many pits have been produced on the surface. The surface preparation parameters, such as Ar partial pressure, Ar ion energy, and oxidation time, have been optimized such that well-defined nanopits with density at $1.09 \times 10^{12}/\text{cm}^2$ and one atom depth could be reproducibly obtained on the etched HOPG surfaces.

An STM image of a 0.13 ML Ag overlayer grown on the etched HOPG surface is given in Figure 1b. It can be seen that most of the Ag particles are located at the pit edges, indicating that the nanopits act as the nucleation sites and result in a relatively narrow size distribution and homogeneous spatial distribution of the Ag particles. From the STM images shown in Figure 1b–h, we see that the particle sizes vary with the Ag coverage. Here, the Ag particle sizes were determined to be ~ 5 nm for 0.13 ML Ag, ~ 7 nm for 0.4 ML Ag, ~ 10 nm for 1.2 ML Ag, ~ 12 nm for 2 ML Ag, ~ 13 nm for 6 ML Ag, ~ 30 nm for 24 ML Ag, and ~ 42 nm for 48 ML Ag. The detailed particle size distribution can be found in Supporting Information Figure S1. It is clear that at large Ag coverage particle coalescence occurs, and some Ag particles can be as large as 90 nm at 48 ML Ag coverage (as shown in Figure 1h). Furthermore, the particle density is also critically dependent on the Ag coverage. For example, the Ag particle density is $1.07 \times 10^{12}/\text{cm}^2$ for the 0.13 ML Ag overlayer, which significantly decreases to $3.69 \times 10^{10}/\text{cm}^2$ at the 48 ML Ag coverage.

In addition, the hexagonal shape of faceted Ag particles can be clearly distinguished from the STM images, which is particularly obvious for the Ag surfaces with large Ag coverage (e.g., Figure 1h). Considering the usual epitaxy relationship of $(111)_{\text{fcc-metal}} \parallel (1000)_{\text{HOPG}}$ for noble metal growth on HOPG,^{16,24}

(20) Hovel, H.; Becker, T.; Bettac, A.; Reihl, B.; Tschudy, M.; Williams, E. J. *J. Appl. Phys.* **1997**, *81*, 154.

(21) Zhu, Y. J.; Hansen, T. A.; Ammermann, S.; McBride, J. D.; Beebe, T. P. *J. Phys. Chem. B* **2001**, *105*, 7632.

(22) Song, Z.; Cai, T. H.; Hanson, J. C.; Rodriguez, J. A.; Hrbek, J. *J. Am. Chem. Soc.* **2004**, *126*, 8576.

(23) Lee, S. M.; Lee, Y. H.; Hwang, Y. G.; Hahn, J. R.; Kang, H. *Phys. Rev. Lett.* **1999**, *82*, 217.

(24) Irawan, T.; Barke, I.; Hovel, H. *Appl. Phys. A: Mater. Sci. Process.* **2005**, *80*, 929.

(19) Yao, Y. X.; Liu, X.; Fu, Q.; Li, W. X.; Tan, D. L.; Bao, X. H. *ChemPhysChem* **2008**, *9*, 975.

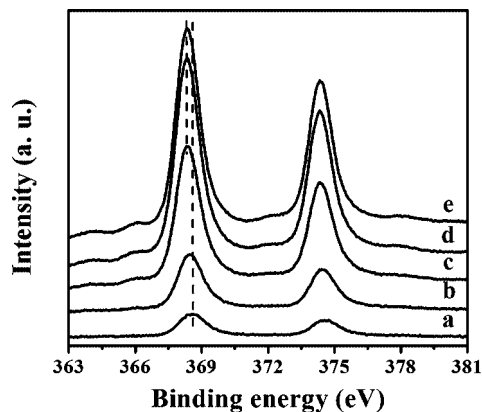


Figure 2. Ag 3d XPS spectra from the Ag particles surfaces grown on HOPG with various coverages: (a) 0.13 ML, (b) 0.4 ML, (c) 1.2 ML, (d) 2 ML, and (e) 6 ML.

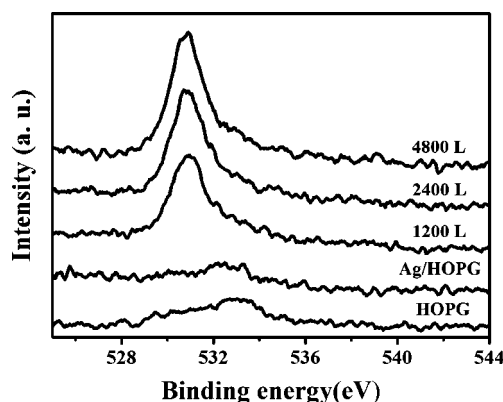


Figure 3. O 1s XPS spectra from the surface of 6 ML Ag particles exposed to different amounts of O₂ at RT.

the Ag particles grown on HOPG should have the main (111) top facets.

We have also studied the Ag overlayers on HOPG by XPS. The Ag 3d spectra from the Ag particle surfaces are displayed in Figure 2, and a binding energy shift of -0.3 eV was observed with increasing Ag coverage. It is known that the interaction between a metal and the carbon support is not strong,¹⁶ which means the binding energy shifts in HOPG supported metal nanoparticles may be attributed to both final state effects,⁵ that is, the weak screening effect in small metal clusters, and initial state effects.¹⁶

3.2. Adsorption of O₂. The surface reactivity of the HOPG supported Ag particles to O₂ was studied by XPS as a function of exposure by monitoring the O 1s spectra. It should be mentioned that a small amount of oxygen signals with the main peak of O 1s at 533.0 eV can be detected on the etched HOPG surfaces and the fresh Ag/HOPG surfaces (Figure 3). This residual oxygen may originate from oxidation of defect sites on the surfaces, which was also reported by Kim and co-workers.²⁵

When exposing the Ag/HOPG surfaces to O₂, an increase in the O 1s intensity was observed. For example, Figure 3 shows the O 1s spectra from the surface of 6 ML Ag particles exposed to different amounts of O₂ at RT. The O 1s signal was found to increase with O₂ exposure, as expected, but does not saturate even after 4800 L O₂. The main peak of the O 1s spectra is now located at 530.8 eV with a small shoulder peak at 533.0 eV. Extensive work has been performed to study O₂ adsorption on

Ag surfaces, primarily focused on single crystal Ag(111),^{26,27} Ag(110),^{28,29} and Ag(001).^{30,31} These works concluded that O₂ can dissociatively adsorb on the low-index Ag crystal surfaces at 300 K. O 1s peaks at 530.3 and 530.4 eV were observed on the O₂-exposed Ag(111) surface, which were attributed to atomic oxygen species of O_β and O_α, respectively.³² Bukhtiyarov et al. studied O₂ adsorption on polycrystalline Ag surfaces, and two O 1s peaks at around 528.4 and 530.5 eV were assigned to the ionic (nucleophilic) oxygen species and the covalent (electrophilic) oxygen species, respectively.^{33,34} Therefore, the observed O 1s feature at 530.8 eV on the O₂ exposed Ag/HOPG surfaces should be from atomic oxygen due to dissociative adsorption of O₂ on the Ag particles.

Similar O₂ adsorption experiments were conducted on various Ag surfaces including the Ag particles with Ag coverage ranging from 0.4 to 48 ML and the bulk Ag(111) surface. The XPS results indicate that O₂ dissociation occurs on all of the Ag surfaces but the amount of the dissociated oxygen varies largely on each surface. For example, strong O 1s peaks can be seen on the O₂-exposed 6 ML Ag/HOPG surface (Figure 3), while little O 1s signal was observed on the Ag(111) surface exposed to the identical amount of O₂. The peak areas of the O 1s signal recorded from various Ag surfaces exposed to 2400 L O₂ are plotted as a function of Ag coverage (Figure 4a). With increasing Ag coverage, the O 1s peak intensity first increases and then decreases after a maximum at 24 ML Ag coverage.

3.3. Adsorption of CHCl₃. Experiments similar to the oxygen adsorption discussed above were performed for CHCl₃ adsorption on the Ag surfaces. CHCl₃ was found to be inert on the bulk Ag(111) surface as evidenced by XPS where there was no detectable Cl species after exposing the surface to CHCl₃ (<48 L). Polanyi and co-workers³⁵ applied Auger electron spectroscopy (AES) to study the reaction of chloromethanes on Ag(111) at RT, and their AES data showed that CHCl₃ had not reacted with Ag(111), which is consistent with our experiments.

Reactions of CHCl₃ on Ag particles are quite different from that on the Ag(111) surface. Figure 5 displays Cl 2p XPS spectra recorded from the Ag particles (2 ML coverage) exposed to different amounts of CHCl₃. A single Cl 2p doublet structure with Cl 2p_{3/2} and 2p_{1/2} centered at 197.9 and 199.4 eV appears after CHCl₃ exposure at RT. The Cl 2p intensity increases with CHCl₃ exposure and does not saturate after 48 L CHCl₃ adsorption. Baetzold has studied CHCl₃ dissociation on Ag clusters supported on carbon films and confirmed the formation of Cl–Ag bonds on the surface.³⁶ Thus, we suggest that the Cl species detected by XPS should be the dissociated Cl bonded to Ag.

Like the O₂ adsorption on Ag surfaces, the CHCl₃ dissociation is also dependent on the Ag surface structure. The areas of Cl 2p peaks from the various Ag surfaces exposed to 24 L CHCl₃

(26) Benndorf, C.; Franck, M.; Thieme, F. *Surf. Sci.* **1983**, *128*, 417.

(27) Demongeot, F. B.; Valbusa, U.; Rocca, M. *Surf. Sci.* **1995**, *339*, 291.

(28) Prince, K. C.; Paolucci, G.; Bradshaw, A. M. *Surf. Sci.* **1986**, *175*, 101.

(29) Vattuone, L.; Rocca, M.; Restelli, P.; Puppo, M.; Boragno, C.; Valbusa, U. *Phys. Rev. B* **1994**, *49*, 5113.

(30) Rocca, M.; Savio, L.; Vattuone, L.; Burghaus, U.; Palomba, V.; Novelli, N.; de Mongeot, F. B.; Valbusa, U.; Gunnella, R.; Comelli, G.; Baraldi, A.; Lizzit, S.; Paolucci, G. *Phys. Rev. B* **2000**, *61*, 213.

(31) Costina, I.; Schmid, M.; Schiechl, H.; Gajdos, M.; Stierle, A.; Kumargurusaran, S.; Hafner, J.; Dorsch, H.; Varga, P. *Surf. Sci.* **2006**, *600*, 617.

(32) Bao, X.; Muhler, M.; SchedelNiedrig, T.; Schlogl, R. *Phys. Rev. B* **1996**, *54*, 2249.

(33) Bukhtiyarov, V. I.; Boronin, A. I.; Savchenko, V. I. *J. Catal.* **1994**, *150*, 262.

(34) Bukhtiyarov, V. I.; Havecker, M.; Kaichev, V. V.; Knop-Gericke, A.; Mayer, R. W.; Schlogl, R. *Phys. Rev. B* **2003**, *67*, 235422.

(35) Dixonwarren, S. J.; Jensen, E. T.; Polanyi, J. C. *J. Chem. Phys.* **1993**, *98*, 5938.

(36) Baetzold, R. C. *J. Am. Chem. Soc.* **1981**, *103*, 6116.

(25) Lim, D. C.; Lopez-Salido, I.; Kim, Y. D. *Surf. Sci.* **2005**, *598*, 96.

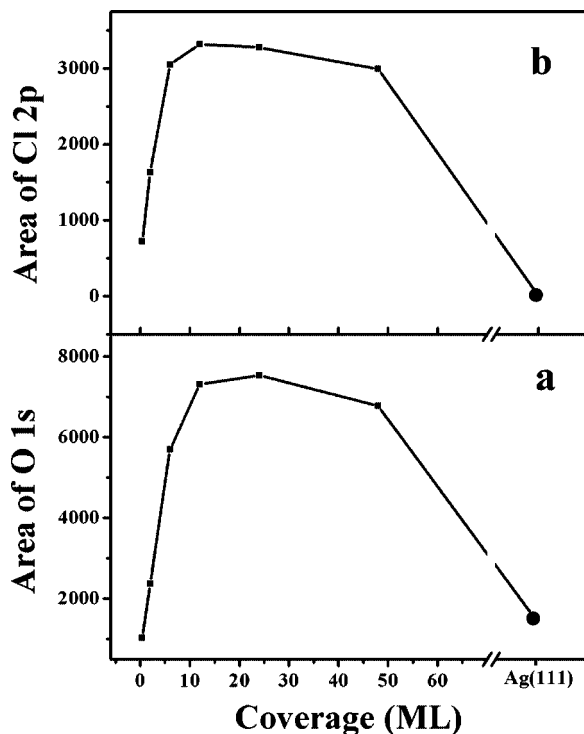


Figure 4. (a) The areas of O 1s peaks from the surfaces of Ag nanoparticles with various Ag coverages exposed to 2400 L O₂; (b) the areas of Cl 2p peaks from the surfaces of Ag nanoparticles with various coverages exposed to 24 L CHCl₃ at RT. The values for the bulk Ag(111) surface are also presented in the figure for comparison (●).

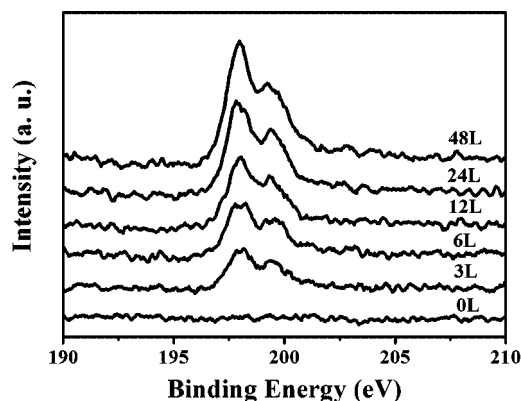


Figure 5. Cl 2p XPS spectra from the surface of 2 ML Ag particles exposed to different amounts of CHCl₃ at RT.

are shown in Figure 4b. In case of the same CHCl₃ exposure (24 L), the amount of surface dissociated Cl species first increases with Ag coverage, and after a turning point at 12 ML Ag coverage it decreases with the increasing Ag coverage.

3.4. Adsorption of CCl₄. We also exposed the different Ag surfaces to CCl₄ and monitored the surface adsorbed or dissociated Cl species by XPS. For example, Figure 6 shows the Cl 2p spectra recorded from 2 ML coverage Ag particles exposed to different amount of CCl₄, where a well-resolved Cl 2p doublet structure with Cl 2p_{3/2} and 2p_{1/2} centered at 197.9 and 199.4 eV is observed. The intensity of the feature increases with CCl₄ exposure and reaches saturation at 24.2 L CCl₄. The surface adsorption of CCl₄ on Ag surfaces has been studied in detail.^{19,37,38}

It was shown that CCl₄ molecularly adsorbs on the Ag(111) surface at 100 K. At elevated temperatures, CCl₄ molecules start to desorb from the surface, while other CCl₄ molecules dissociate into dichlorocarbene, :CCl₂, and atomic Cl species. Two :CCl₂

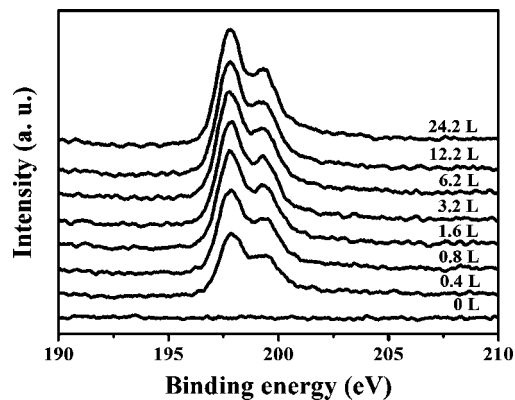


Figure 6. Cl 2p XPS spectra from the surface of 2 ML Ag particles exposed to different amounts of CCl₄ at RT.

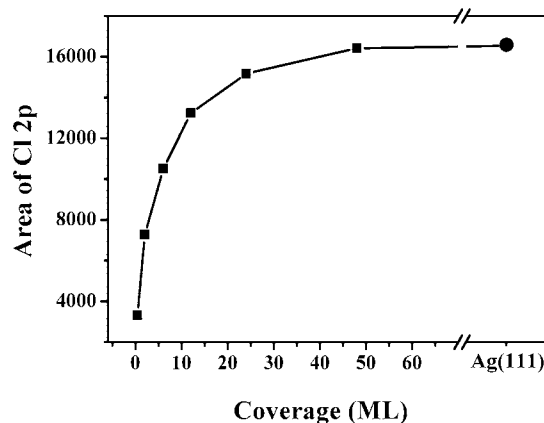


Figure 7. Areas of Cl 2p peaks from the surfaces of Ag nanoparticles with various Ag coverages exposed to 24.2 L CCl₄ at RT. The value for the bulk Ag(111) surface is also presented in the figure for comparison (●).

species can react with each other to form C₂Cl₄, which desorb almost completely at 250 K, leaving behind chemisorbed Cl species on the Ag(111) surface. In our experiment, we observed only one Cl species with XPS (Figure 6), which can be attributed to the atomic Cl bonded with surface Ag.^{39,40} Thus, it can be concluded that CCl₄ dissociatively adsorbs on Ag particles at RT, producing atomic Cl chemisorbed on Ag.

The CCl₄ dissociation reaction was found to occur on both the surfaces of the Ag particles and the Ag(111) surface. In contrast to O₂ and CHCl₃, strong CCl₄ dissociation was observed on the bulk Ag(111) surface. As shown in Figure 7, the amount of the dissociated Cl keeps on increasing with the Ag coverage and reaches a maximum on the Ag(111) surface upon the same CCl₄ exposure at 24.2 ML.

3.5. Reaction Mechanism of O₂, CHCl₃, and CCl₄ on Ag. The reactions of O₂, CHCl₃, and CCl₄ on the Ag surfaces all show significant size-dependence (see Figures 4 and 7), but the effect of the Ag particle size on the surface reactivity varies significantly with the adsorbed molecules. Strong reactions of CCl₄ occur on the defect-free bulk Ag(111) surface, suggesting that this reaction does not require surface defect sites. Weak dissociation reactions happen for O₂ and CH₃Cl adsorption on

(37) Dixonwarren, S. J.; Jensen, E. T.; Polanyi, J. C. *Phys. Rev. Lett.* **1991**, *67*, 2395.

(38) Bovet, N.; Sayago, D. I.; Allegretti, F.; Kroger, E. A.; Knight, M. J.; Barrett, J.; Woodruff, D. P.; Jones, R. G. *Surf. Sci.* **2006**, *600*, 241.

(39) Piao, H.; Adib, K.; Chang, Z.; Hrbek, J.; Enever, M.; Barteau, M. A.; Mullins, D. R. *J. Phys. Chem. B* **2003**, *107*, 13976.

(40) Medlin, J. W.; Barteau, M. A. *Surf. Sci.* **2002**, *506*, 105.

the bulk Ag(111) surface, while strong reactions take place on Ag particles with medium coverage. The results indicate that the surface reactions of O₂ and CHCl₃ on Ag are structure-sensitive but structure-insensitive for CCl₄ surface reactions, which leads to very different reaction mechanisms.

The concept that the surface defects, such as atomic steps and point defects, act as the “active sites” in catalytic reactions has been known for many years.^{41–43} It has been shown that O₂ adsorption on Ag surfaces is dependent on the Ag crystal plane and the density of surface defects. For example, at 300 K oxygen adsorbs dissociatively on Ag(111) with a sticking coefficient of $S_0 \approx 10^{-5}$,²⁶ which is 2 orders of magnitude lower than that of a Ag(110) surface.⁴⁴ On a Ag(001) surface, the nanostructuring morphology increases the O₂ dissociation probability from less than 10⁻³ on a flat surface to 0.1 on the rippled surface.⁴⁵ Therefore, it is expected that the defect-free Ag(111) surface presents low reactivity to O₂ dissociation, and this is what we see here (Figure 4a). In contrast, Ag particles have many surface defects, such as facets, edges, and corners, which provide active sites for O₂ dissociative adsorption. The number of defect sites on the surface of the Ag particles depends on the Ag coverage. In the range of low Ag coverage, an increase in the Ag coverage will increase the particle density and size, bringing more defect sites on the surface. After certain Ag coverage, strong particle coalescence will decrease the particle density and the number of surface defect sites. The volcano-type dependence of the amount of dissociated oxygen species with the Ag coverage (Figure 4a) suggests that the surface defect sites play a critical role in the O₂ dissociation reactions on Ag. The Ag surface with a medium coverage having the largest number of surface defect sites demonstrates the highest reactivity to O₂.

The situation of CHCl₃ adsorption on the Ag surfaces is quite similar to that of O₂. On the perfect Ag(111) surface, little CHCl₃ dissociation occurs due to the low surface defect density. On Ag particles surfaces, the probability for the CHCl₃ dissociative reaction first increases and then decreases as the Ag coverage increases (Figure 4b). The results indicate that the dissociation of CHCl₃ on Ag is also controlled by the number of surface defect sites.

CCl₄ reactions on Ag surfaces are totally different from the other molecules studied. Here, we observed strong reactions occurring on the bulk Ag(111) surface (Figure 7). The reaction mechanism of CCl₄ on Ag was explored by Bovet et al., and it was suggested that CCl₄ adsorption on Ag happens with three chlorine atoms bonded with three surface Ag atoms with the fourth C–Cl bond aligned with the surface normal.³⁸ The unit mesh size of Ag(111) is 2.89 Å, which is almost equal to the 2.85 Å Cl–Cl separation in molecular CCl₄, which suggests that the flat Ag(111) surface could serve as the active site for CCl₄ dissociation. Furthermore, our density functional theory calculation shows that activation energy for the C–Cl bond dissociation on Ag(111) is as low as 0.19 eV.¹⁹ The available results confirm that the CCl₄ dissociation on Ag is structure-insensitive and it is the Ag(111) facet surface area rather than the number of surface defect sites that determines the CCl₄ dissociation reaction. Thus, it can be understood that the bulk Ag(111) surface presenting large surface area demonstrates strong CCl₄ dissociation reactions (Figure 7).

4. Conclusion

Nanopits with one atomic depth can be prepared on the HOPG surfaces by Ar⁺ sputtering in UHV and oxidation in air. The pits acting as nucleation sites for Ag particles make it possible to prepare Ag particles with various sizes ranging from 5 to 90 nm. Reactions of O₂, CHCl₃, and CCl₄ on the Ag particles and bulk Ag(111) surfaces demonstrate different size-dependent behaviors. Strong CCl₄ dissociation occurs on the Ag(111) surface where it is structure-insensitive, and the extent of dissociation is determined by the Ag(111) facet surface area. Quite weak O₂ and CHCl₃ dissociation reactions were observed on the bulk Ag surfaces, while strong reactions happen on Ag nanoparticles with medium Ag coverage. The reactions of O₂ and CHCl₃ on Ag surfaces were controlled by the number of surface defect sites.

Acknowledgment. This work was financially supported by the National Natural Science Foundation of China (No. 90206036, No. 20573107, and No. 20603037), Ministry of Science and Technology of China, and Chinese Academy of Sciences. We owe warm thanks to Dr. Jason White for critical reading of this manuscript.

Supporting Information Available: Diagrams of particle size distribution of Ag particles with coverages of 0.13, 0.4, 1.2, 2, 6, 24, and 48 ML (Figure S1). This material is available free of charge via the Internet at <http://pubs.acs.org>.

LA801348N

(41) Yates, J. T. *J. Vac. Sci. Technol.* **1995**, *13*, 1359.

(42) Zambelli, T.; Wintterlin, J.; Trost, J.; Ertl, G. *Science* **1996**, *273*, 1688.

(43) Hammer, B. *Phys. Rev. Lett.* **1999**, *83*, 3681.

(44) Bowker, M.; Barteau, M. A.; Madix, R. J. *Surf. Sci.* **1980**, *92*, 528.

(45) Costantini, G.; de Mongeot, F. B.; Rusponi, S.; Boragno, C.; Valbusa, U.; Vattuone, L.; Burghaus, U.; Savio, L.; Rocca, M. *J. Chem. Phys.* **2000**, *112*, 6840.